EIS AFM FEI tBLMs Langmuir 2010

DATASET · OCTOBER 2012

7 AUTHORS, INCLUDING:

David J Vanderah

Institute for Bioscience and Biotechnology R…

90 PUBLICATIONS   **1,846** CITATIONS

SEE PROFILE

Thomas B Parr

University of Delaware

38 PUBLICATIONS   **45** CITATIONS

SEE PROFILE

Curtis W Meuse

National Institute of Standards and Technol…

64 PUBLICATIONS   **1,307** CITATIONS

SEE PROFILE

Gintaras Valincius

Vilnius University

82 PUBLICATIONS   **1,086** CITATIONS

SEE PROFILE

Formation and Finite Element Analysis of Tethered Bilayer Lipid Structures

Kwang Joo Kwak,[†,‡] Gintaras Valincius,[§] Wei-Ching Liao,[†,||] Xin Hu,[†] Xuejin Wen,[†,⊥] Andrew Lee,[#] Bo Yu,[†,‡] David J. Vanderah,[▽] Wu Lu,[†,⊥] and L. James Lee*,[†,‡]

[†]NSF Nanoscale Science and Engineering, Center for Affordable Nanoengineering of Polymeric Biomedical Devices (NSEC-CANPBD), [‡]Department of Chemical and Biomolecular Engineering, The Ohio State University, Columbus, Ohio 43210, United States, [§]Institute of Biochemistry, Vilnius University, Mokslininku 12, LT-08662 Vilnius, Lithuania, [||]Department of Mechanical Engineering, and [⊥]Department of Electrical and Computer Engineering, The Ohio State University, Columbus, Ohio 43210, United States, [#]School of Electrical and Computer Engineering, Georgia Institute of Technology, Atlanta, Georgia 30332, United States, and [▽]Macromolecular Structure and Function Group at the Institute of Bioscience and Biotechnology Research (IBBR), National Institute of Standards and Technology (NIST), Rockville, Maryland 20850, United States

Rapid solvent exchange of an ethanolic solution of diphytanoyl phosphatidylcholine (DPhyPC) in the presence of a mixed self-assembled monolayer (SAM) [thiolipid/β-mercaptoethanol (βME) (3/7 mol/mol) on Au] shows a transition from densely packed tethered bilayer lipid membranes [(dp)tBLMs], to loosely packed tethered bilayer lipid membranes [(lp)tBLMs], and tethered bilayer liposome nanoparticles (tBLNs) with decreasing DPhyPC concentration. The tethered lipidic constructs in the aqueous medium were analyzed by atomic force microscopy (AFM) and electrochemical impedance spectroscopy (EIS). Finite element analysis (FEA) was applied to interpret spectral EIS features without referring to equivalent circuit modeling. Using structural data obtained earlier from neutron reflectometry and dielectric constants of lipid bilayers, we reproduced experimentally observed features of the electrochemical impedance (EI) spectra of complex surface constructs involving small pinhole defects, large membrane-free patches, and bound liposomes. We demonstrated by FEA that highly insulating (dp)tBLMs with low-defect density exhibit EI spectra in the shape of a perfect semicircle with or without low-frequency upward "tails" in the Cole−Cole representation. Such EI spectra were observed at DPhyPC concentrations of $>5 \times 10^{-3}$ mol L^{-1}. While AFM was not able to visualize very small lateral defects in such films, EI spectra unambiguously signaled their presence by increased low frequency "tails". Using FEA we demonstrate that films with large diameter visible defects (>25 nm by AFM) produce EI spectral features consisting of two semicircles of comparable size. Such films were typically obtained at DPhyPC concentrations of $<5 \times 10^{-3}$ mol L^{-1}. At DPhyPC concentrations of $<1.0 \times 10^{-3}$ mol L^{-1} the planar bilayer structures were replaced by ellipsoidal liposomes with diameters ranging from 50 to 500 nm as observed in AFM images. Despite the distinct surface morphology change, the EI curves exhibited two semicircle spectral features typical for the large size defects in planar tBLMs. FEA revealed that, to account for these EI features for bound liposome systems (50−500 nm diameter), one needs to assume much lower tBLM conductivities of the submembrane space, which separates the electrode surface and the phospholipid bilayer. Alternatively, FEA indicates that such features may also be observed on composite surfaces containing both bound liposomes and patches of planar bilayers. Triple semicircular features, observed in some of the experimental EI curves, were attributed to an increased complexity of the real tBLMs. The modeling demonstrated that such features are typical for heterogeneous tBLM surfaces containing large patches of different defectiveness levels. By integrating AFM, EIS, and FEA data, our work provides diagnostic criteria allowing the precise characterization of the properties and the morphology of surface supported bilayer systems.

Introduction

Bilayer lipid structures such as membranes are vital constructs in cell biology as they form the boundaries between the intracellular cytoplasm and the extracellular environment and thus are the host sites of many of the drug targets of the pharmaceutical industry. The dynamic nature of material transport across the native cell membranes is difficult to understand due to the complexity of the membranes and the phenomenon.[1] Recent advances in tethered biomimetic lipid membranes provide opportunities to study protein adsorption, ion transport, and membrane mechanical properties[2−4] as well as to develop applications such as biosensing, drug delivery, biocatalysis, and cellular recognition.[5−16] Such lipid membranes may provide a generic platform for biosensor devices.[17−19] The mechanism of tethered bilayer lipid membrane

*To whom correspondence should be addressed. Mailing address: 140 W. 19th Ave, Columbus, OH 43210, USA. Phone: 614-292-2408. E-mail: lee.31@osu.edu.

(1) Vereb, G.; Szollosi, J.; Matko, J.; Nagy, P.; Farkas, T.; Vigh, L.; Matyus, L.; Waldmann, T. A.; Damjanovich, S. *Proc. Natl. Acad. Sci. U.S.A.* **2003**, *100*, 8053.
(2) Schmidt, A.; Spinke, J.; Bayerl, T.; Sackmann, E.; Knoll, W. *Biophys. J.* **1992**, *63*, 1385.
(3) Sackmann, E. *Science* **1996**, *271*, 43.
(4) Williams, L. M.; Evans, S. D.; Flynn, T. M.; Marsh, A.; Knowles, P. F. R.; Bushby, J.; Boden, N. *Langmuir* **1997**, *13*, 751.

(5) Plant, A. L. *Langmuir* **1993**, *9*, 2764.
(6) Lang, H.; Duschl, C.; Vogel, H. *Langmuir* **1994**, *10*, 197.
(7) Raedler, J.; Strey, H.; Sackmann, E. *Langmuir* **1995**, *11*, 4539.
(8) Keller, C. A.; Kasemo, B. *Biophys. J.* **1998**, *75*, 1397.
(9) Cornell, B. A.; Krishna, G.; Osman, P. D.; Pace, R. D.; Wieczorek, L. *Biochem. Soc. Trans.* **2001**, *29*, 613.
(10) Ekeroth, J.; Konradsson, P.; Hoeoek, F. *Langmuir* **2002**, *18*, 7923.
(11) Krishna, G.; Schulte, J.; Cornell, B. A.; Pace, R. J.; Osman, P. D. *Langmuir* **2003**, *19*, 2294.
(12) Reimhult, E.; Hoeoek, F.; Kasemo, B *Langmuir* **2003**, *19*, 1681.
(13) Schiller, S. M.; Naumann, R.; Lovejoy, K.; Kunz, H.; Knoll, W. *Angew. Chem.* **2003**, *42*, 208.
(14) Richter, R. P.; Brisson, A. R. *Biophys. J.* **2005**, *88*, 3422.
(15) Thompson, D. H. *ACS Nano* **2008**, *2*, 821.
(16) Mintzer, M. A.; Simanek, E. E. *Chem. Rev.* **2009**, *109*, 259.
(17) Cornell, B. A.; Braach-Maksvytis, V. L. B.; King, L. G.; Osman, P. D. O.; Raguse, B.; Wieczorek, L.; Pace, R. J. *Nature* **1997**, *387*, 580.
(18) Tanaka, M.; Sackmann, E. *Nature* **2005**, *437*, 656.
(19) Daniel, S.; F. Albertorio, F.; Cremer, P. S. *MRS Bull.* **2006**, *31*, 536.

(tBLM) formation on the gold substrates was investigated by Dorvel et al.[20] using a quartz crystal microbalance (QCM) and visualized by an atomic force microscope (AFM). They proposed deposition pathways for the formation of lipid monolayers, then bilayer formation by vesicle fusion. Another study showed the formation of tBLMs by the fusion of liposomes from phospholipids via self-assembled monolayers (SAMs) of a thiolipid.[21]

Using tBLMs,[22−26] the interactions between proteins and membranes were investigated by electrochemical impedance spectroscopy (EIS) and neutron reflection (NR) measurements for a broad range of biomedical applications such as toxicology and Alzheimer's disease.[23,25,26] In these works, it was demonstrated that NR may provide structural details of tBLMs along the surface normal with the resolution of several angstroms.

Even though EIS demonstrates exceptional sensitivity to the presence of lateral irregularities and defects (natural or artificially induced) in tBLMs,[22] the question of whether and to what extent EIS data may provide details of the structural organization and physical properties of tBLMs is not adequately addressed. Until now, there had been few attempts to relate the physical properties of tBLMs and experimental EIS spectra.[11,17] It was demonstrated that the finite element (Supporting Information in ref 17) and ladder-type distributed network[11] analyses provide the possibility to retrieve physical data from EIS, e.g., to make estimates of the conductance of the submembrane space separating the phospholipid bilayer and the solid surface by only 1−2 nm. In most cases, complex-shaped EI spectra observed in experiments are fitted to the model equivalent circuits of different complexities. However, even though good fits may be obtained, the physical meaning of the elements used to construct the equivalent circuits and their relation to the physical properties of tBLMs is vague.

In this study, we aim to establish correlations between the experimental EI spectra and the geometry and physical properties of tBLMs. We chose a tethered membrane system characterized earlier[22] by EIS and NR, which can be readily formed by the solvent exchange procedure. We found that by varying the phospholipid concentration in the organic solvent, which in the course of tBLM preparation is replaced by an aqueous buffer, various surface phospholipid structures, from bilayers containing nanoholes to anchored vesicles, may be produced, resulting in characteristic features in the EIS spectra. In this work, we reproduce those features by using finite element analysis (FEA) without referring to the electric equivalent circuit modeling. FEA requires knowledge of the morphology and the geometry of an object. Therefore, we applied AFM to visualize the in-plane structural features of the tBLMs. The experimental visualization of soft

materials by AFM is now a well-established technology.[27−39] In combination with other electrochemical techniques, it was used to probe electric-field effects,[40] the bilayer formation process,[20,41] and the combination of AFM and polarized total internal reflection fluorescence microscopy.[42]

Experimental[43]

Materials. Synthesis and purification of the 1-thiahexa(ethylene oxide) lipidic anchor molecule WC14 [20-tetradecyloxy-3,6,9,12,15,18,22-heptaoxahexatriacontane-1-thiol], was described previously.[22] The phospholipid, 1,2-diphytanoyl-*sn*-glycero-3-phosphocholine (DPhyPC), was used as supplied from Avanti Polar Lipids (Birmingham, AL). β-Mercaptoethanol (βME) from Sigma-Aldrich (St. Louis, MO) was distilled before use. Distilled water was obtained from a HQ grade water purification system at The Ohio State University (Columbus, OH). An aqueous solution of phosphate buffered saline (PBS) with 137 mM[44] NaCl, 2.7 mM KCl, 10 mM Na_2HPO_4, 2 mM KH_2PO_4, and a pH of 7.4 was used after dilution from $10 \times$ PBS (Thermo Scientific, Rockford, IL). Thin Au layers (20 nm) over a Ti adhesion layer ($\sim$ 2 nm) were deposited at a deposition rate of 0.02 nm/s on Si $\langle 100 \rangle$ wafer using a Denton vacuum E-beam evaporator (DV-502A; Moorestown, NJ). The Au layers typically had a surface roughness (rms) of 0.2 nm ± 0.1 nm, as measured by AFM (Asylum Research, Santa Barbara, CA).

Preparation of the Densely Packed tBLM [(dp)tBLM], Loosely Packed tBLM [(lp)tBLM], and Tethered Bilayer Liposome Nanoparticle (tBLN) Constructs. The anchoring membrane mixed SAMs were formed on smooth, flat Au layers as described previously.[22] Briefly, the freshly prepared Au films were exposed to solutions of WC14:βME (3:7 mol:mol, 0.2 mM total concentration) in 99.5% ethanol for >12 h. The bilayer lipid structures were then prepared by incubation of the SAMs with DPhyPC solutions of 10, 5, 3, 2, 1, 0.6, 0.3, or 0.1 mM in ethanol for ~10 min followed by vigorous injection of PBS buffer within ~10 s leading to the formation of planar (dp)- or (lp)tBLMs or spherical tBLNs.

Atomic Force Microscopy. AFM was performed in the PBS buffer solution using a MFP-3D-Bio-AFM (Asylum Research, Santa Barbara, CA) equipped with an *i*Drive Magnetic Actuated Cantilever holder. The fluid cell was sonicated in ethanol for 5 min before use, immediately followed by extensive rinsing with ethanol and drying under a stream of N_2 gas. Images were

(20) Dorvel, B. R.; Keizer, H. M.; Fine, D.; Vuorinen, J.; Dodabalapur, A.; Duran, R. S. *Langmuir* **2007**, *23*, 7344.

(21) Naumann, R.; Schiller, S. M.; Giess, F.; Grohe, B.; Hartmann, K. B.; Kärcher, I.; Köper, I.; Lübben, J.; Vasilev, K.; Knoll, W. *Langmuir* **2003**, *19*, 5435.

(22) McGillivray, D. J.; Valincius, G.; Vanderah, D. J.; Febo-Ayala, W.; Woodward, J. T.; Heinrich, F.; Kasianowicz, J. J.; Lösche, M. *Biointerphases* **2007**, *2*, 21.

(23) Valincius, G.; McGillivray, D. J.; Febo-Ayala, W.; Vanderah, D. J.; Kasianowicz, J. J.; Lösche, M. *J. Phys. Chem. B* **2006**, *110*, 10213.

(24) Heinrich, F.; Ng, T.; J. Vanderah, D. J.; Shekhar, P.; Mihailescu, M.; Nanda, H.; Lösche, M. *Langmuir* **2009**, *25*, 4219.

(25) Valincius, G.; Heinrich, F.; Budvytyte, R.; Vanderah, D. J.; McGillivray, D. J.; Sokolov, Y.; Hall, J. E.; Lösche, M. *Biophys. J.* **2008**, *95*, 4845.

(26) McGillivray, D. J.; Valincius, G.; Heinrich, F.; Robertson, J. W.; Vanderah, D. J.; Febo-Ayala, W.; Ignatjev, I.; Lösche, M.; Kasianowicz, J. J. *Biophys. J.* **2009**, *96*, 1547.

(27) Butt, H. J.; Cappella, B.; Kappl, M. *Surf. Sci. Rep.* **2005**, *59*, 1.

(28) Connell, S. D.; Smith, D. A. *Mol. Membr. Biol.* **2006**, *23*, 17.

(29) Richter, R. P.; Berat, R.; Brisson, A. R. *Langmuir* **2006**, *22*, 3497.

(30) Leroueil, P. R.; Hong, S.; Mecke, A.; Baker, J. R.; Orr, B. G.; Holl, M. M. B. *Acc. Chem. Res.* **2007**, *40*, 335.

(31) Seantier, B.; Giocondi, M.-C.; Le Grimellec, C.; Milhiet, P.-E. *Curr. Opin. Colloid Interface Sci.* **2008**, *13*, 326.

(32) Goksu, E. I.; Vanegas, J. M.; Blanchette, C. D.; Lin, W.-C.; Longo, M. L. *Biochim. Biophys. Acta, Biomembr.* **2009**, *1788*, 254.

(33) El Kirat, K.; Morandat, S.; Dufrene, Y. F. *Biochim. Biophys. Acta, Biomembr.* **2010**, *1798*, 750.

(34) Zhang, L.; Vidu, R.; Waring, A. J.; Lehrer, R. I.; Longo, M. L.; Stroeve, P. *Langmuir* **2002**, *18*, 1318.

(35) Chen, M.; Li, M.; Brosseau, C. L.; Lipkowski, J. *Langmuir* **2009**, *25*, 1028.

(36) Burns, A. R. *Langmuir* **2003**, *19*, 8358.

(37) Feng, Z. V.; Spurlin, T. A.; Gewirth, A. A. *Biophys. J.* **2005**, *88*, 2154.

(38) Steltenkamp, S.; Mueller, M. M.; Deserno, M.; Hennesthal, C.; Steinem, C.; Janshoff, A. *Biophys. J.* **2006**, *91*, 217.

(39) Fukuma, T.; Higgins, M. J.; Jarvis, S. P. *Phys. Rev. Lett.* **2007**, *98*, 106101.

(40) Jeuken, L. J. C. *Biophys. J.* **2008**, *94*, 4711.

(41) Vockenroth, I. K.; Rossi, C.; Shah, M. R.; Köper, I. *Biointerphases* **2009**, *4*, 19.

(42) Oreopoulos, J.; Epand, R. F.; Epand, R. M.; Yip, C. M. *Biophys. J.* **2010**, *98*, 815.

(43) Certain commercial materials, pieces of equipment, and instruments are identified in this manuscript in order to specify the experimental procedure as completely as possible. In no case does such identification imply a recommendation or endorsement by the National Institute of Standards and Technology, nor does it imply that the materials, equipment, or instruments identified are necessarily the best available for the purpose.

(44) The accepted SI unit of concentration, mol/L, has been represented by the symbol M in order to conform to the conventions of this journal.

acquired using the AC Mode in fluid, collected using a scan rate of 0.5 Hz and a resonant frequency of 5−6 kHz with the set point of 0.1−0.2 V (90−80% reduced from free amplitude of the AFM cantilever) unless specified otherwise. Au-coated Si_3N_4 pyramidal cantilevers with a nominal spring constant of 0.09 N/m (AR-*i*Drive-N01, Asylum Research) were mounted in the fluid cell. SPIP software (Scanning Probe Image Processor, Image Metrology A/S, Denmark) was used to analyze the surface roughness and characterize the particles and pores based on their size and shape.

Electrochemical Impedance Spectroscopy. EIS measurements were performed using an electrochemical impedance system (Gamry Instruments, Warminster, PA, model Series G300 potentiostat, EIS300 software). The spectra were obtained for frequencies between 0.1 and 3×10^5 Hz with 10 logarithmically distributed measurements per decade. Four electrochemical cells were assembled on a 20 mm × 40 mm large Au-coated silicon wafer used as the working electrode that had the tBLMs/tBLNs attached to its surface. Each of these four parallel cells had a geometric surface area (A_{el}) of 0.126 cm². All EIS data were normalized to A_{el}. The reference was a saturated silver−silver chloride (Ag/AgCl/KCl(aq,sat)) microelectrode (1004G, Koslow Scientific Co., Englewood, NJ), and the auxiliary electrode was a 0.5 mm diameter platinum wire (Aldrich, St. Louis, MO, 99.99% purity) coiled around the barrel of the reference electrode. All measurements were carried out at 0 V direct current (DC) bias and 30 mV alternating current (AC) versus reference electrode at 21 ± 1 °C.

Finite Element Analysis. The basis for the FEA simulation in the AC field[45−47] is the following equation:

$$\nabla \cdot ((\sigma + j\omega\varepsilon)\nabla\tilde{\phi}) = \frac{\partial\rho}{\partial t} \qquad (1)$$

where σ and ε are the conductivity and permittivity of the medium, $j = \sqrt{-1}$, $\omega = 2\pi f$ is the angular frequency, f is the frequency in hertz, $\tilde{\phi}$ is the complex voltage, and ρ is the free (unpaired) charge density. We further denote $\tilde{\sigma} = \sigma + j\omega\varepsilon$. Under steady-state conditions, the current density lines neither originate nor terminate inside the conducting system, thus eq 1 reduces to

$$\nabla \cdot (\tilde{\sigma}\nabla\tilde{\phi}) = 0 \qquad (2)$$

The computational domain is a cylinder defined by radius R and height h. Axial symmetry is applied so that any point within and on the surface of a cylinder is defined by coordinates z and r, which are the coordinates along the normal to the base and the radius, respectively. Therefore, the dimensionality of the problem is reduced from 3 to 2. The wall of the cylinder is assumed to act as an ideal insulator, which means that the current density normal to the wall is zero. The cylinder bases are assumed to be equipotential and kept at $\tilde{\phi}$ (h,r) = constant (top) and $\tilde{\phi}$ (0,r) = 0 (grounded bottom). The cylinder is assumed to be filled with an electrolyte. The top base is assumed to be a surface of an ideally nonpolarizable electrode, meaning that the impedance of the interface between the solution and the electrode is zero (i.e., to a first approximation, the Ag/AgCl interface in direct contact with high free chloride concentration solutions may be regarded as an ideally nonpolarizable electrode). The bottom base of the cylinder is assumed to be a working gold electrode covered by a SAM, tBLMs, or other self-assembled entities considered in this work. A more detailed cross-section view of the surfaces is discussed further.

(45) Calame, J. P. *J. Appl. Phys.* **2003**, *94*, 5945.
(46) Sun, T.; Green, N. G.; Morgan, H. *Nano: Brief Rep. Rev.* **2008**, *3*, 55.
(47) Cattarin, S.; Musiani, M.; Tribollet, B.; Vivier, V. *Electrochim. Acta* **2009**, *54*, 6963.

The complex current density $\tilde{J}$ enters the cylinder at the top base and drains through the bottom base. Due to the specific arrangement of the conducting phases in the system, the current density at $z = h$ is uniform, so it is equivalent for all r. Consequently, the ultimate goal is to find the impedance $\tilde{Z}$ of the system for the parameter ω value:

$$\tilde{Z}(\omega) = \frac{\tilde{\phi}(h,r)}{\tilde{J}(h,r)} \qquad (3)$$

where

$$\tilde{J}(h,r) = \tilde{\sigma}(h,r)\nabla\tilde{\phi}(h,r) \qquad (4)$$

The complex current density at any point (z,r), including (h,r) could be found by solving eq 2 with respect to $\nabla\tilde{\phi}$ (h,r). This is done using the commercial FEA software COMSOL (COMSOL, Inc., Burlington, MA) with the AC module. Equation 2 is solved at each node with imposed boundary conditions, and the condition of the continuity of electric current is strictly observed.

In this work, the EIS data are presented in the form of Cole−Cole plots, and are therefore calculated in accordance with eq 2; $\tilde{Z}(\omega)$ values are transformed into the complex capacitance $\tilde{C}(\omega)$ as follows:

$$\tilde{C}(\omega) = \frac{1}{j\omega\tilde{Z}} \qquad (5)$$

The corresponding real versus imaginary plot of $\tilde{C}(\omega)$ constitutes the EIS spectra in the Cole−Cole representation. The calculations were carried out for 41 logarithmically equally spaced points covering the frequency range from 1×10^{-2} to 10^6 Hz.

Results and Discussion

AFM of tBLMs and tBLNs. Figure 1a−f shows AFM images of lipid configurations obtained at DPhyPC concentrations, hereafter designated as [DPhyPC], of 10, 5, 3, 1, 0.6, and 0.3 mM, respectively, after thorough rinsing with PBS buffer. (dp)tBLMs were observed at [DPhyPC] ≥ 5 mM (Figure 1a,b), with small lipid structures on top that increased the calculated surface roughness (rms) to 0.6 ± 0.1 nm and 0.9 ± 0.2 nm, respectively. In the 10 mM [DPhyPC] case, many large and small liposomes were observed on top of the (dp)tBLMs prior to rinsing (photos not shown; average diameter of the liposomes was about 100 nm from a profile image). These liposomes on the planar (dp)tBLMs increased the surface roughness to about 10 nm (rms) and, in most cases, could be easily relocated by the AFM tip at very high normal loads (90%-reduced from free amplitude of the cantilever) [0.1 V; data not shown].

At [DPhyPC] = 3 mM and 1 mM (Figure 1c,d, respectively), the lipid configuration changes from (dp)tBLMs to (lp)tBLMs containing nanoscale pores. The pore depth was 6.1 ± 0.7 nm, equivalent to the bilayer lipid thickness, while the measured lateral pore size spanned from ∼50 to 500 nm. Surface roughness was 1.5 ± 0.3 and 2.8 ± 0.5 nm, respectively. The AFM-measured pore size was dependent on the normal load (set point of the AFM cantilever amplitude), indicating the lower packing density of the DPhyPC in the bilayers and weak forces at defect (pore) edges. Often, AFM scans show smaller than actual pore sizes due to tip radius effects. On the other hand, the destructive action by an AFM tip, especially on the edges of the defects, tends to physically make the pores larger. Because lipid bilayers are soft, the second effect may be dominant, and, consequently, the AFM-measured pores seen in Figure 1c,d could be slightly larger than the actual size. Interestingly, AFM captured the existence of surface regions
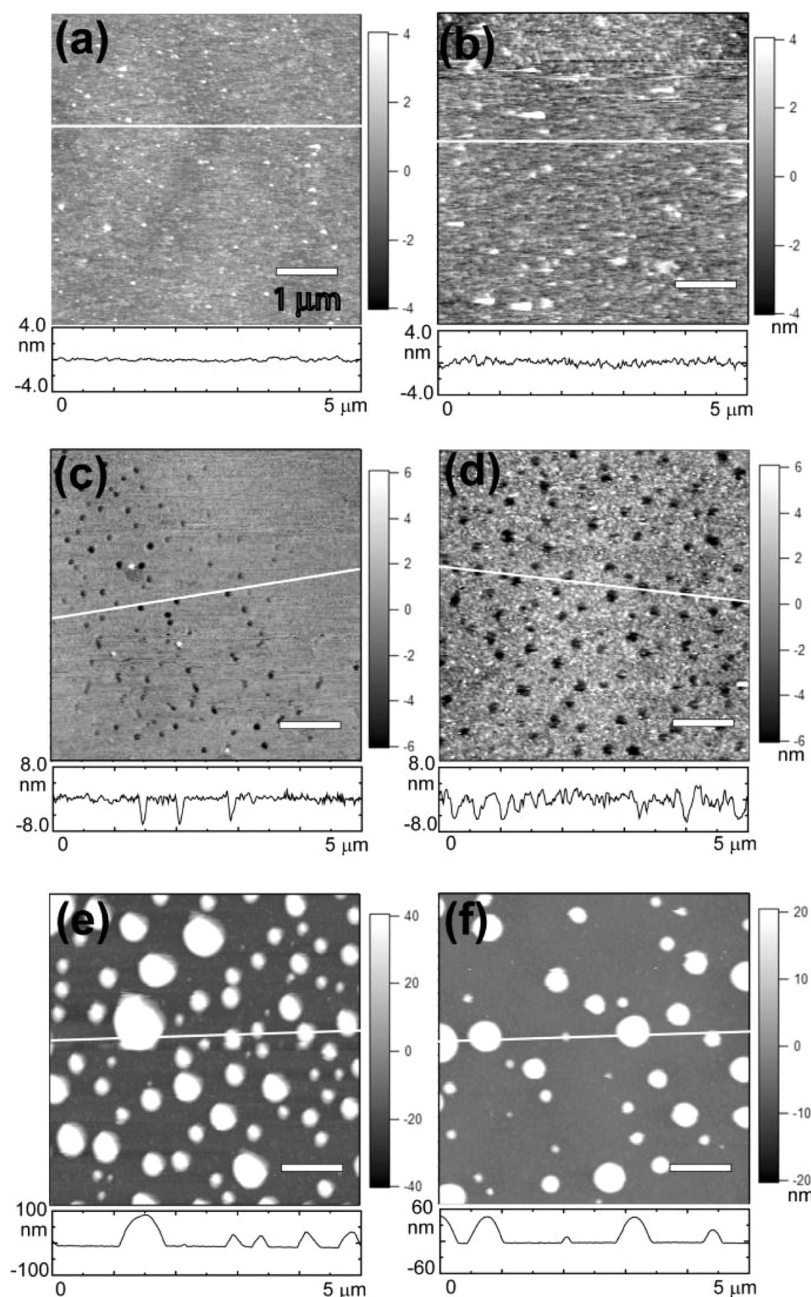
Figure 1. AFM images and cross sectional profiles with scan sizes of 5 μm $\times$ 5 μm obtained in aqueous medium at (a) 10, (b) 5, (c) 3, (d) 1, (e) 0.6, and (f) 0.3 mM DPhyPC concentration. The white lines indicate the locations of the cross sections. In each AFM image, the vertical bar shows the scale of the *z*-axis, in which the maximum means a threshold value the same as the white color above that.

with different defect levels at higher [DPhyPC]s. In Figure 1c, one may clearly distinguish a defect-free patch in the upper right corner of the figure, while the other section of the AFM scan is populated with 50−200 nm defects.

The lipidic configuration changed dramatically at [DPhyPC] < 1 mM. Instead of lipid membranes, the structure changed to spherical tBLNs (Figure 1e,f; [DPhyPC]s = 0.6 mM and 0.3 mM, respectively, with corresponding surface roughness of 22.4 $\pm$ 2.1 nm and 13.7 $\pm$ 1.1 nm). Because liposomes in direct contact with a solid surface tend to deform, flatten, or rupture,[48,49] we attribute the stability and shape of these tBLNs to the presence of the thiolipid anchor, WC14. The roughness of the surface including

the tBLNs is calculated by vertical deviation of the entire surface and is different from the average height of the liposomes (60.6 $\pm$ 5.4 nm). At [DPhyPC] $\leq$ 0.6 mM, AFM shows that planar BLMs were replaced by liposomes with lateral diameters ranging from 50 to 500 nm. The shape of the liposomes resembles an oblate spheroid, with major and minor axes equal to 200 and 60 nm, respectively. The tip-induced artifacts in the AFM images come from the dependence of the lateral size. That is, sharper tips can more accurately measure actual sizes since the contact area between the tip and the sample is smaller. The lateral size of an AFM sample is usually overestimated due to the tip radius, so in order to correct for this error, the tip radius may be subtracted from the AFM measurement. For example, if the AFM tip radius is 20 nm, then 40 nm may be subtracted from the measured size in order to estimate the actual size of the sample. On the other hand, the height in AFM

(48) Vermette, P. *Methods Enzymol.* **2009**, *465*, 43.
(49) Yu, B.; Lee, R. J.; Lee, L. J. *Methods Enzymol.* **2009**, *465*, 129.
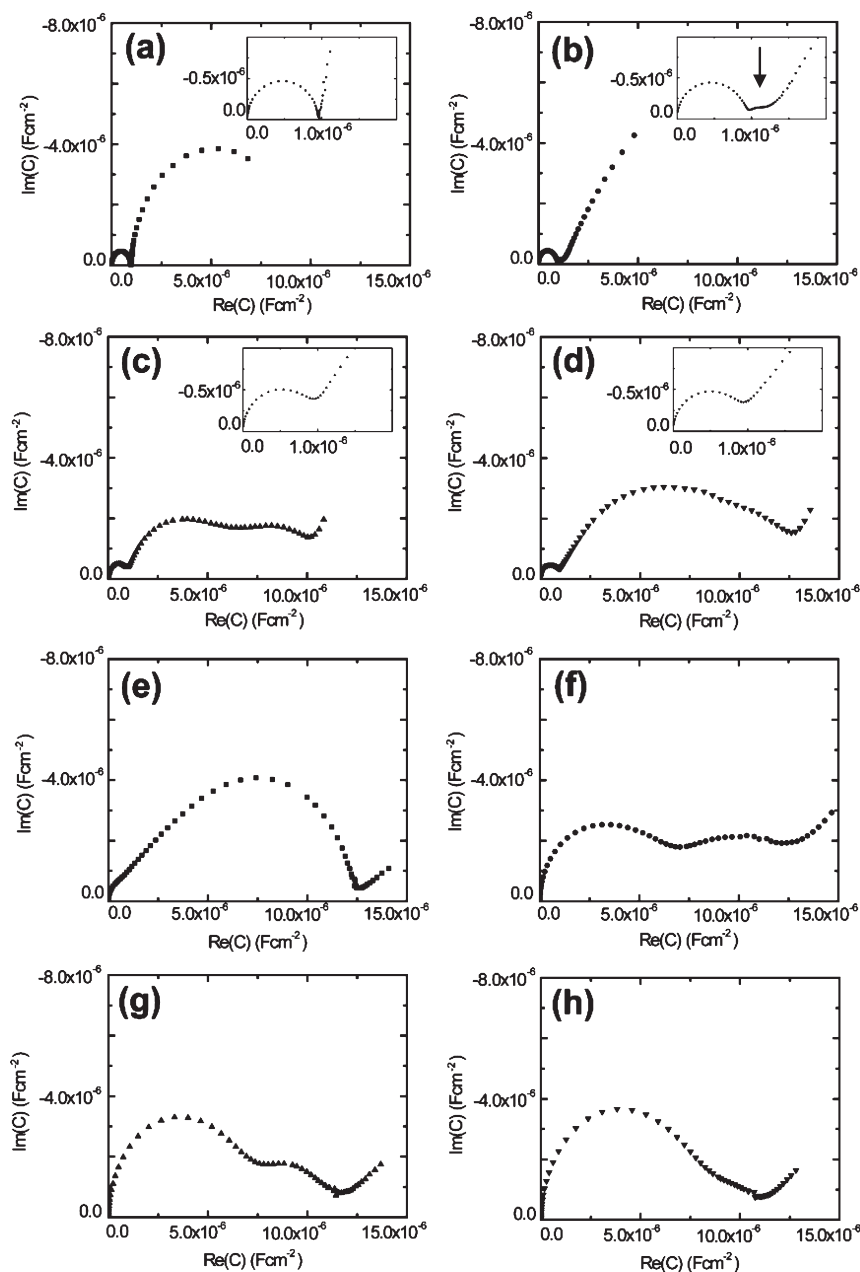
Figure 2. Cole−Cole plots of the EI spectra, normalized to A_{el}, of the corresponding tethered lipid bilayers at DPhyPC lipid concentrations of (a) 10, (b) 5, (c) 3, (d) 2, (e) 1, (f) 0.6, (g) 0.3, and (h) 0.1 mM. Insets to the figures show expanded views of the EIS data. The arrow in the inset of panel b is discussed later with the arrow in Figure 7b.

images is underestimated because of the deformation of the sample from the vertical pressure during the scanning. Even with consideration of these the lateral size and height artifacts, the difference between a major axis and a minor axis of an oblate spheroid is still large. Further elucidation of the process on the formation of the tethered liposomes is needed in order to discern the formation of the asymmetric structure of the bound liposomes.

EIS of tBLMs and tBLNs. Figure 2a−h shows Cole−Cole plots from the electrochemical impedance (EI) spectra of the lipid configurations obtained from [DPhyPC] of 10, 5, 3, 2, 1, 0.6, 0.3, and 0.1 mM, respectively. Upon tBLM formation at [DPhyPC] ≥ 5 mM, the changes in the EI spectra are consistent with those expected in converting a tethering SAM (monolayer) to a tBLM (bilayer). The creation of an insulating hydrophobic layer in this process leads to a decrease of the surface capacitance by about a factor of 10, from approximately 10 to 1 μF/cm^2 (without taking

the surface roughness factor into account). The Cole−Cole plots in Figure 2a,b ([DPhyPC] = 10 mM and 5 mM, respectively) display semicircular shapes in the high frequency range and long tails at lower frequencies. The semicircular diameter of EIS plots is proportional to the capacitance of bilayers.[22]

At [DPhyPC] = 3 mM and 2 mM (Figure 2c,d, respectively), the semicircular shape of the EI spectra becomes incomplete, and the low frequency tails become more complex and is attributed to increased conductance pathways in the tBLM. The general features observed in Figure 2c,d suggest an increasing number of nanoscale defects or nanopores. For example, similar EI spectra were observed in complete tBLMs subject to pore forming α-hemolysin toxin[26] and tBLMs partially digested by the membrane phospholipase A$_2$, PLA$_2$,.[23]

Further decrease of the [DPhyPC] to 1 and 0.6 mM leads to the EI spectral changes shown in Figure 2e,f, respectively. The

small, high frequency semicircle in the Cole−Cole plot disappears, concurrent with the development of either one large semicircular shape curve (Figure 2e) or two considerable size semicircular features (Figure 2f). These types of spectra were also observed upon digestion of compact tBLMs by PLA$_2$.[23]

Finally, lowering the [DPhyPC] to <0.3 mM led to further development of the EI spectra into a large single semicircle (Figure 2h) in which the lower frequency branch moves toward the value of that of the tethering SAM only (~10−12 μF/cm^2). In some cases, the lower frequency branch exhibited a propensity to form a residual smaller semicircular feature (Figure 2g), similar to those seen in EI spectra on liposome-free surfaces (Figure 2c,d).

Comparing the observed changes in the EI spectra (Figure 2) to the AFM images (Figure 1) leads to certain interpretations of physical phenomena responsible for the evolution of the EI plots upon decrease of [DPhyPC]. At high concentrations, above 5 mM, the AFM indicates quite uniform surfaces with no visible dents, holes, concavities, etc. This allows us to presume that densely packed tBLMs (obtained at [DPhyPC] > 5 mM) may have defects, whose sizes are below the resolution of the AFM. Given that the typical size of an AFM probe is about 20 nm, we may safely assume that defects of diameter larger than 20 nm do not exist, or they are rare in the tBLMs produced at [DPhyPC] > 5 mM. In this situation, we might expect highly electrically insulating tBLMs with the dielectric properties close to freestanding black lipid membranes. Indeed, the spectra in Figure 2a,b indicate that the tBLM capacitances are close to 1 μF/cm^2 (normalized to the geometric surface area), while the residual conductivity measured from the electrode admittance did not exceed 10−20 μS cm^2 (data not shown).

The comparison of the EI spectra and AFM images obtained for 1 mM ≤ [DPhyPC] < 5 mM suggests that the appearance of relatively large phospholipid uncovered holes (50−400 nm diameter) on the surface triggers either lifting of the small semicircle branch of EI spectrum off the Re C axis (Figure 2c,d) or its merging into the large semicircular feature on the EI curves. Notably, the size and relative density of the pinholes clearly correlate with the extent to which the small, high-frequency part of the EI spectra is affected. Small, low-density defects partially covering the surface area seen in Figure1c ([DPhyPC] = 3 mM) just slightly lift the high frequency semicircular part of the EI spectrum in Figure 2c. Conversely, the high-density, large (up to 400 nm) holes seen in Figure 1d ([DPhyPC] = 1 mM) lead to the disappearance of this feature from the EI spectrum in Figure 2e.

Finally, AFM reveals that at [DPhyPC] < 1 mM, the liposome population may be free or nearly free from the bilayer surface of the precursor SAM. Such a surface should exhibit EI spectra close to that of the pure anchoring SAM, i.e., a single semicircle of 10−12 μF/cm^2 (the roughness factor of the electrode unaccounted) in the Cole−Cole plot.[22] In contrast to the pure membrane precursor SAM, we might expect some blockage of the surface by the oblate liposomal constructs, clearly visible in Figure 1e,f. Indeed, spectra similar to that of the pure mixed SAM are seen in Figure 2g,h. However, Figure 2f displays a specific double semicircular-shaped EI spectrum that differs significantly from the precursor SAM spectrum. It is worth mentioning that while studying liposome fusion on hydrophobic compact SAMs, Silin et al. reported the formation of surface-bound liposomes[50] but claimed that the liposome binding minimally affects the capacitance and the shape of EI spectra. This suggests that, in our studies, the liposomes may be bound by a

different force, presumably from a higher binding affinity due to the specific properties of the precursor SAM made with the lipid-like WC14 molecules. It is possible that the blockage of the surface may be very high in our case. Currently there are no experimental means to confirm or reject such a presumption. Alternatively, it could be that the surfaces partially covered by liposomes may still contain scattered patches of intact tBLMs not visible on AFM images (see Figures 1e,f) due to significantly different z-heights.

Taken all together, AFM analysis of the phospholipid entities formed on the precursor SAM surface can provide some insight into the geometry of tBLM structures formed under different conditions. It may also allow further interpretation of some of the experimentally observed EI spectral features. Nevertheless, such interpretations remain speculative unless there is an independent way to verify them.

Model EI Spectra: Conformity with Experiments. We applied FEA to reconstruct and compare EI spectra with those obtained experimentally. The cross-section of the cylinder conductor and the geometric parameters of the conducting/insulating layers are shown in Figure 3.

We set the following constants for a planar four-layer system in Figure 3a: thickness of the hydrophobic core of insulating bilayer d_{hc} = 3.2 nm (estimated by NR in ref 22) and thickness of the submembrane water-containing reservoir d_{res} = 1.6 nm (ibid). The thickness of the Helmholtz layer d_H was set at 1.6 nm, a value equal to the ellipsometric thickness of a dry precursor (30:70 WC14:βME) SAM. While this value may seem high for the thickness of the SAM in the water environment, one needs to take into account the fact that the dielectric properties of the planar insulating layer are determined not by thickness but by the ratio $\varepsilon'/d = C/\varepsilon_0$ where ε' and ε_0 are the relative dielectric and vacuum permittivities, respectively. Since the specific capacitance value for the precursor SAM is well-established, ~10 μF/cm^2, for an effective surface area with a roughness factor of about 1.4,[22,23,25] we set the relative dielectric permittivity ε'_H = 18, so that the capacitance of the Helmholtz layer would be 10 μF/cm^2.[22] The relative dielectric permittivity of the diphytanolyl hydrophobic layer was set to ε'_{hc} = 2.2.[25] Finally, we set the value of the submembrane reservoir conductivity σ_{res} = 1 × 10^{-5} S/cm, which is ~1000-fold lower than the specific conductivity of PBS used in the current work. This value selection took into account the detailed experimental study performed by Krishna et al.,[11] in which they demonstrated that the conducting properties of a thin layer of electrolyte confined between the gold surface and the phospholipid bilayer are quite different from those of the bulk solution. The same group of researchers claimed[11,17] that the conductance of the submembrane reservoir should be at least 3 orders of magnitude lower in comparison to a bulk electrolyte solution. In the current work, we did not aim for perfect quantitative matches between the experimental results and FEA models; instead, we sought qualitative accord. After an analysis of possible σ_{res} from 1×10^{-2} to 10^{-10} S/cm, we found that the value of 1×10^{-5} S/cm provided the best qualitative fit, in accord with refs 11 and 17. Finally, the thickness and conductivity of the solution d_{sol} and σ_{sol} were kept constant throughout simulation, and were set to 3 mm and 1 × 10^{-2} S/cm, respectively. The distance between the reference/auxiliary and working electrodes in our experimental setup was set at d_{sol} = 3 mm, while σ_{sol} = 1 × 10^{-2} S/cm was approximately equal to the specific conductivity of 0.1 M PBS at pH 7.0, and 20 °C.

The geometry of the planar membrane system in Figure 3a is characterized by two radii: r_0, the radius of a membrane defect; and R, the defect domain radius equal to that of a cylinder analyzed by

(50) Silin, V. I.; Wieder, H.; Woodward, J. T.; Valincius, G.; Offenhausser, A.; Plant, A. L. *J. Am. Chem. Soc.* **2002**, *124*, 14676.
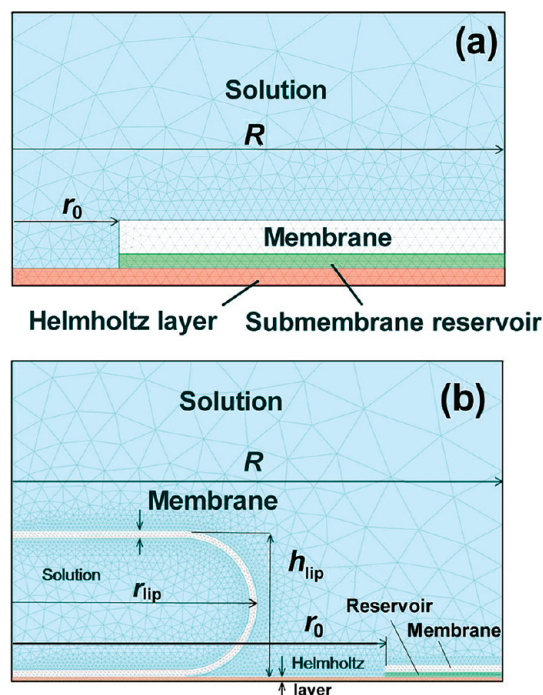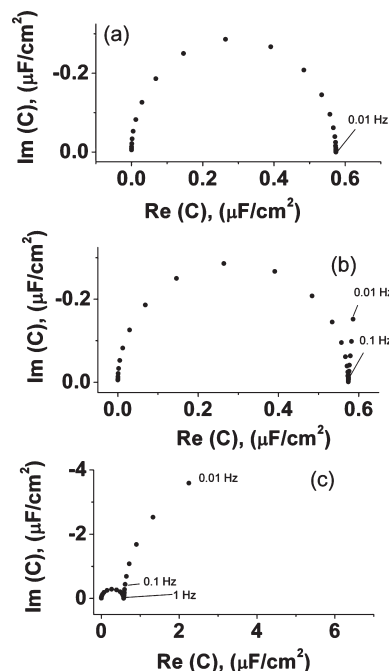
Figure 3. Geometry of the system analyzed by FEA. The mesh was generated by COMSOL. (a) Planar tBLM system is characterized by the radius r_0, which determines the size of the surface patch not covered by the bilayer membrane (defect). It is assumed that the defect is filled with an electrolyte that has the same properties as the bulk electrolyte. R is the radius of the circle that hosts a single defect. The electrolyte properties of the submembrane layer may be significantly different (see Results and Discussion in the text) due to confined space and the presence of the oligo(ethylene oxide) chains of anchoring SAM. The thicknesses of the membrane and the submembrane layer were inferred from neutron reflectivity data, and the parameters of the Helmholtz layer, which is the layer separating the underlying metal and electrolyte, are inferred from capacitance data published elsewhere.[22] (b) Schematics of a composite surface system containing both liposome (tBLN) and surface patches covered by the membrane (tBLM). Liposome radius r_{lip} and liposome height h_{lip} determines the radius of the contact between the surface and the liposome. Because h_{lip} was set to 60 nm, the radius of the contact was equal to $(r_{lip} - 30)$ nm. By setting $r_0 = R$, one may model the situation in which the surface is populated by liposomes (tBLNs) only. By setting $r_{lip} < r_0 \neq R$, one may model the situation in which the surface contains both liposomes (tBLNs) and planar patches of the tBLM.

the FEA method. Also, R determines the surface density of defects $N \approx 1/\pi R^2$, which is a variable parameter in the model.[51] The liposome system is shown in Figure 3b. Its geometry is characterized by the liposome radius, r_{lip}, and liposome height, h_{lip}, while other parameters have the same notations as in the planar system.

Low Defect Density (dp)tBLM Systems. We started FEA with the ideal solid supported bilayer, setting the radius of a defect to $r_0 = 0$, and $R = 1000$ nm. As expected, the Cole−Cole plot of an ideal bilayer exhibits an ideal semicircular shape, arching over the Re (C) axis of the spectrum, with the low frequency limit of $\sim 0.55 \, \mu F/cm^2$ in Figure 4a. Since the Helmholtz layer capacitance was set to $10 \, \mu F/cm^2$, one easily retrieves the capacitance of the hydrophobic core of the tBLM as $0.61 \, \mu F/cm^2$, which agrees well with specific capacitance values for solvent-free black lipid

(51) The actual density is smaller and depends on the type of lateral packing of the model cylinder and the area of the void spaces between cylinders. In the case of the close-packed circle structure, the density is lower by a factor of 0.907.

(52) Redwood, W. R.; Pfeiffer, F. R.; Weisbach, J. A.; Thompson, T. E. *Biochim. Biophys. Acta* **1971**, *233*, 1.

Figure 4. Cole−Cole plots modeled by FEA in highly insulating (dp)tBLM systems. Modeling parameters: $d_{sol} = 3$ mm, $d_{hc} = 3.2$ nm, $d_H = 1.6$ nm, $d_{res} = 1.3$ nm, $\sigma_{sol} = 0.01$ S/cm, and $\sigma_{res} = 10^{-5}$ S/cm. Frequency range is from 1×10^{-2} to 10^6 Hz. (a) $r_0 = 0$ nm, $R = 1000$ nm; (b) $r_0 = 1$ nm, $R = 50000$ nm, defect density $\sim 0.0001 \, \mu m^{-2}$; (c) $r_0 = 1$ nm, $R = 10000$ nm, defect density $0.003 \, \mu m^{-2}$.
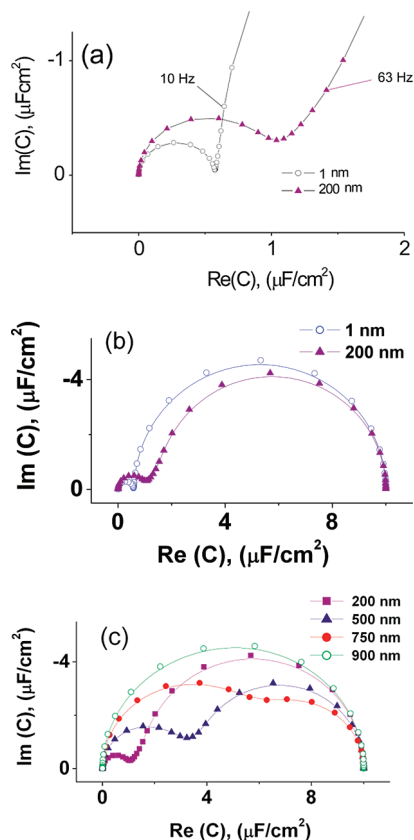
DPhyPC membranes.[52] FEA shows that small (1 nm) water-filled pinholes in tBLMs do not change EI spectra until their density reaches values of 1×10^{-4} to $3 \times 10^{-3} \, \mu m^{-2}$, at which a second large arch, whose radius depends on the conductivity of ionic reservoir σ_{res}, starts to develop (see Figure 4b,c). Notably, the frequency at which this new feature starts to appear in the EI spectra is a good diagnostic criterion of the defectiveness of the tBLMs. If the bounce back of the complex capacitance curve from the Re (C) axis does not start above ~ 0.1 Hz (Figure 4b), one may expect the defect density to be below $1 \times 10^{-4} \, \mu m^{-2}$, which is comparable to the single-channel recording conditions in black lipid membranes. As the density of defects increases, this frequency point also increases (see Figure 4c). Another important criterion for small size and low defect densities in tBLMs is the closeness of the EI spectrum curve to the Re (C) axis in the frequency range of the reversal. Both criteria are not significantly affected by the variation in the defect size up to an $r_0 \sim 50$ nm, at least, not to the extent the spectral changes could be detected experimentally. Therefore, comparing the model tBLM spectra in Figure 4a−c and the experimental tBLM spectra in Figure 2a,b, we may conclude that very compact tBLMs with low defect density below AFM resolution are formed at [DPhyPC] > 5 mM. Most likely, defect sizes are from 1 to 20 nm with densities smaller than 3×10^{-3} to $3 \times 10^{-1} \, \mu m^{-2}$. Even though the AFM is not capable of detecting such small pinholes in the membrane in Figure 1a,b, their presence is clearly manifested in the EI spectra in Figure 2a,b.

High Defect Density (lp)tBLM Systems. The dilution of [DPhyPC] below 5 mM leads to the formation of visible round holes in tBLMs (Figure 1c,d). FEA data (Figure 5a) indicate that the main feature attesting to the increase of the size of the defects is a detachment and drift off the Re (C) axis of the complex capacitance extremum. In addition, its shape changes from the sharp-edge (Figure 5a, open circles, $r_0 = 1$ nm) to a

Figure 5. Cole−Cole plots modeled by FEA in poorly insulating (lp)tBLM systems. Modeling parameters: d_{sol} = 3 mm, d_{hc} = 3.2 nm, d_H = 1.6 nm, d_{res} = 1.3 nm, σ_{sol} = 0.01 S/cm, σ_{res} = 10^{-5} S/cm, R = 1000 nm, and fixed defect density ∼ 0.3 μm^{-2}; r_0 values are indicated on charts. (a) small defects, high and mid-frequency range of the spectrum; (b) small defects, whole frequency range spectrum from 1×10^{-2} to 10^6 Hz; (c) large defects, whole frequency range from 1×10^{-2} to 10^6 Hz.

rounded-shape as the defect size increases (Figure 5a, triangles, r_0 = 200 nm). On the larger scale, the EI curves transform into double semicircular spectra with a smaller semicircle located in the high-frequency part of the spectrum (see Figure 5b). We emphasize here that the appearance of the black spots on the AFM images in Figure 1c,d is followed by the upward shift of the extremum point from the Im (C) axis in the experimental EIS curves. This shift is clearly visible in the insets of Figure 2c,d. Since the FEA predicts such evolutions of the EI spectra, one may conclude that the AFM images (Figure 1c,d) capture the existence of round defects formed in the membranes during the solvent exchange, but not an artifact introduced by the AFM tip in the course of imaging.

Another important feature that evolves with the increasing defect size is a total transformation of the high frequency part of the spectra. A general feature of this transformation is a significant increase in the size of the previously small high frequency semicircle, typically used[22−26] to assess the capacitance of the phospholipid membrane in low defect density tBLMs. According to data in Figure 5c, once the defect radius increases to a level that the uncovered precursor SAM patches reach >25−50% of the total electrode surface, the EI curves transform into double semicircles, with one becoming bigger while the other at the low frequency end shrinks (Figure 5c, triangles and solid circles). Upon further defect radius increase to 900 nm, which is equivalent to ∼75% (in close-packed two-dimensional (2D) structures) surface coverage by the membrane-free patches (Figure 5c, open

circles), two semicircles merge into a single one. This means that the remaining 25% of the surface patches covered by phospholipid bilayer now provide no electrical insulation to the electrode. Consequently, the resulting capacitive semicircle at the low frequencies hits the Re (C) axis at the value of the Helmholtz layer capacitance of an anchoring SAM (10 $\mu F/cm^2$ in this model). Such model predicted features displayed in Figure 5 are seen in experimental EI spectra (Figure 2e−g) of tBLM structures obtained at [DPhyPC]s between 1.0 and 0.3 mM. Surprisingly, at [DPhyPC] < 1.0 mM, the AFM morphology of the surface drastically changes; the surface becomes populated by tBLNs. However, the model spectrum shown in Figure 5c (solid circles), even though resembling general features of the spectrum shown in Figure 2g, was generated without taking into account the presence of tBLNs on the surface.

Tethered Liposomes (tBLN) Systems. To resolve this disparity, we applied FEA to surfaces that may contain both tBLNs and tBLM. First, using the schematics shown in Figure 3b, we set the parameters r_0 = R, which means that the surface contains only tBLNs, while the rest of the electrode is homogeneously covered by the precursor SAM. The vesicle size (r_{lip} = 150 nm), density (R = 200 nm, which is equivalent to a density ∼7 μm^{-2} in the close-packed configuration), and the attachment mode (squeezed oblate spheroid) to a surface were chosen in such a way that ∼33% of the surface would be tightly blocked intact tBLN, as shown in Figure 3b, and the area of contact would not contain a water reservoir. The resulting EI spectrum is a single semicircle, whose size is smaller in comparison to a Helmholtz capacitance of the surface [Figure 6a (solid circles)]. The decrease of the semicircle size to ∼6.6 $\mu F/cm^2$ is a direct consequence of a blockage of the surface by the tBLN. Modification of the modeling conditions and allowing a water reservoir with conductance σ_{res} = 10^{-5} S/cm to fill the gap between the attached vesicle and the SAM only increased the size of the semicircular spectrum to a 10 $\mu F/cm^2$ Helmholtz layer [Figure 6a (open circles)]. In both cases, the model does not compare favorably with the experimentally recorded spectra (Figure 2f−h) that exhibit double semicircular features. FEA modeling indicates that in order to reproduce these features one needs to assume that the submembrane space exhibits conductance much lower than that of a water-filled reservoir in the tBLMs. Figure 6a (solid and open squares) demonstrates that decreasing the conductivity to σ_{res} = 10^{-7} S/cm yields a double semicircular feature to the modeled EI spectra. Such low reservoir conductivity in our tBLN systems is an open question. Upon binding, our tBLNs trigger significant EI spectral changes in contrast to the previous work by Silin et al.,[50] who reported vesicle binding without EI spectral changes. This indicates a much higher electrical insulating property of the tBLNs, suggesting a tighter contact with the underlying anchoring SAM. Notably, at σ_{res} = 10^{-7} S/cm, one may reproduce the subtle experimental EI spectral variations seen in Figure 2g,h. As the density of the vesicles decreases (Figure 1e,f), the EI spectra (Figure 2f−h) indicate a consistent decrease of the radius of the semicircle in the low frequency range. FEA replicates this trend. Figure 6b demonstrates the development of the EI spectra upon the decrease of the vesicle density from 7 to 3.2 μm^{-2}. Decrease of the liposome density to zero will transform the EI spectra into the clean precursor SAM spectrum, which is a single semicircle with 10 $\mu F/cm^2$ radius (data not shown).

The analysis of modeled spectra evolution with the liposome size (data not presented) and the defect density (Figure 6b) suggests that the size of the low frequency semicircular part of the EI is proportional to the surface fraction blocked by the bound liposomes. Consequently, this may serve as a diagnostic
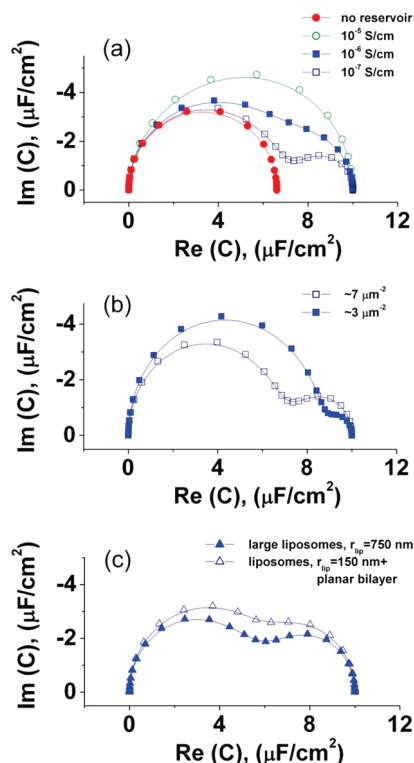
Figure 6. FEA generated Cole−Cole plots in tBLN systems. (a) Liposomes on the surface, r_{lip} = 150 nm, r_0 = R = 200 nm (no planar bilayer patches), liposome density $\sim$7 μm^{-2}; the dependence of EI spectra on the submembrane reservoir conductivity: solid circles - no reservoir; open circles - σ_{res} = 10^{-5} S/cm; solid squares - σ_{res} = 10^{-6} S/cm; open squares - σ_{res} = 10^{-7} S/cm. (b) Liposomes on the surface, r_{lip} = 150 nm, r_0 = R, σ_{res} = 10^{-7} S/cm; the dependence of EI spectra on liposome density: solid squares - 3 μm^{-2} (R = 300 nm); open squares - 7 μm^{-2} (R = 200 nm). (c) Comparison of EI spectra of large liposomes and composite surface: solid triangles - liposome only with r_{lip} = 750 nm, r_0 = R = 1000 nm, σ_{res} = 10^{-5} S/cm, liposome density $\sim$0.3 μm^{-2}; open triangles - composite surface with r_{lip} = 150 nm, r_0 = 750 nm, R = 1000 nm, σ_{res} = 10^{-5} S/cm, liposome density $\sim$0.3 μm^{-2}. All plots are in the frequency range from 1$\times$10^{-2} to 10^6 Hz.

criterion for either size or density of bound liposomes. The experimental EI spectrum in Figure 2f indicates two semicircular features of comparable sizes, while the AFM detects the presence of bound liposomes at [DPhyC] = 0.6 mM. This suggests that the blocked surface fraction is $\sim$50%. Reproducing such a situation in FEA modeling by increasing the liposome densities beyond $\sim$7 μm^{-2} seems less realistic given the experimental densities observed by AFM. As an alternative, we increased the vesicle size to reproduce the proportions of the semicircular features seen in Figure 2f. FEA modeling assuming σ_{res} = 10^{-5} S/cm required an increase of r_{lip} to 750 nm (contact radius -720 nm) and fixing R = 1000 nm, which is equivalent to $\sim$47% blockage of the surface (closed-packed 2D structure). This leads to the development of the double semicircular features of comparable sizes [Figure 6c (solid triangles)] reproducing the main features of the plot in Figure 2g. However, in our case, the experimentally measured lateral radii of the vesicles were typically smaller (25−250 nm), suggesting that large vesicles are unlikely to account for the double semicircle features in Figure 2g.

Smaller vesicles from 50 to 500 nm can give rise to double semicircular spectra if they are bound to surfaces partly covered by patches of tBLMs. We modeled such a situation by applying FEA to a composite surface (Figure 3b) containing tBLNs (r_{lip} =
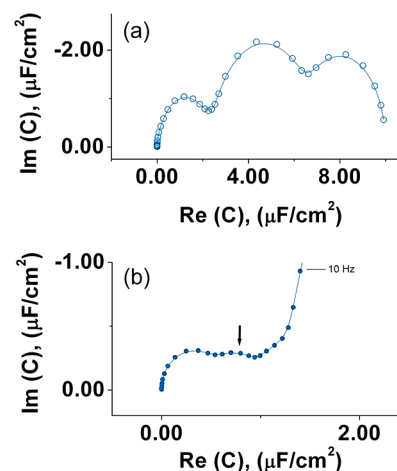

Figure 7. Modeled Cole−Cole plots of composite surfaces obtained using eq 6. Modeling parameters: d_{sol} = 3 mm, d_{hc} = 3.2 nm, d_H = 1.6 nm, d_{res} = 1.3 nm, σ_{sol} = 0.01 S/cm, and σ_{res} = 10^{-5} S/cm. (a) Small defects: r_0 = 1 nm, R = 1000, defect density $\sim$0.3 μm^{-2}, surface fraction −37%; large defects: r_0 = 500 nm, R = 1000, defect density $\sim$0.3 μm^{-2}, surface fraction −63%, and frequency range from 1 × 10^{-2} to 10^6 Hz. (b) Small defects: r_0 = 10 nm, R = 1000, defect density $\sim$0.3 μm^{-2}, surface fraction −93%; large defects: r_0 = 750 nm, R = 1000, defect density $\sim$0.3 μm^{-2}, surface fraction −7%, frequency range from 10 to 10^6 Hz.

150 nm, $\sim$ 2% surface coverage by liposomes) and partly covered by tBLM (r_0 = 750 nm, $\sim$ 50% coverage by the planar bilayer). This resulted in the EI spectrum shown in Figure 6c (open triangles) that closely reproduced the features in Figure 2g. It is quite possible that at [DPhyC] from 1.0 to 0.6 mM, at which the transition from the planar defective membrane to bound vesicle systems occurs, there may coexist both lipid structures on the surface. From this, it follows that at least three surface features may cause the Cole−Cole EI spectra to develop into double semicircular curves: (i) small liposomes with radii $\sim$150 nm and low conductivity (10^{-7} S/cm) submembrane reservoir (Figure 6a,b), (ii) large liposomes with surface contact radii > $\sim$720 nm along with high conductivity (10^{-5} S/cm) of the submembrane reservoir [Figure 6c (solid triangles)], and (iii) liposomes and planar tBLM patches simultaneously present on the surface [Figure 6c (open triangles)].

Complex Surfaces Composed of Different Defect Density Patches. Until now, several spectral features were skipped from our analysis because we could not account for them by the straightforward application of the FEA according to the scheme in Figure 3a. One of these is a triple semicircle visible in the Figure 2c spectrum obtained at [DPhyC] = 3 mM. Amazingly, at the very same concentration, the AFM captured a complex surface morphology consisting of both a featureless and likely defect-free region, and tBLM regions populated with defects. If the size of the regions is significantly larger than the defects themselves, as is obviously the case in Figure 1c, then neglecting boundary effects, we may calculate the complex capacitance of such a composite surface as a linear combination of the capacitances of densely (small defects) and loosely packed (large defects) tethered bilayers according to the formula:

$$C_{composite} = \theta_{dp}C_{dp} + \theta_{lp}C_{lp} \qquad (6)$$

where θ_{dp} and θ_{lp} are the fractions occupied by densely and loosely packed surface areas, respectively, and C_{dp} and C_{lp} are the corresponding specific capacitances. To qualitatively reproduce the spectrum of Figure 2c, we carried out FEA on a surface composed of two areas: 37% of (dp)tBLMs and 63% of
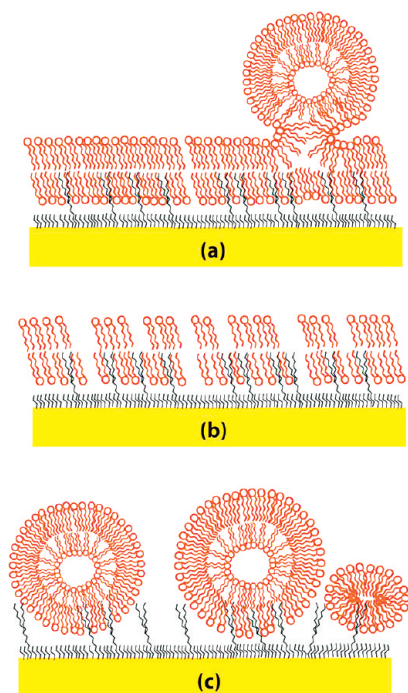
Figure 8. Schematics of (a) (dp)tBLMs with the small defects, (b) (lp)tBLMs, and (c) tBLNs.

(lp)tBLMs. The former is populated with tiny 1 nm radius defects that, in our case, are beyond the detection limits of AFM, and the latter is populated with big defects (500 nm diameter holes). This generated the EI spectrum (Figure 7a), which displays the triple semicircle feature seen in the experimental spectrum (Figure 2c), with the only difference at the very low frequency edge (this is discussed further).

Another spectral feature that may be reconstructed using eq 6 is seen in the experimental spectrum in the inset of Figure 2b. While the semicircular spectrum of highly insulating tBLMs tends to touch the Re (C) axis as the frequency decreases (Figure 2a, inset), closer inspection of the spectra reveals a slight lift off the axis and the formation of a flat transition region between the high-frequency semicircle and the mid-frequency ascending EI curve. This feature is marked in Figure 2b inset with an arrow. We have generated similar flat features in model spectra using eq 6. Figure 7b shows the flat transition region, from FEA on a surface consisting of 93% of (dp)tBLMs, populated with 10 nm radius defects, and 7% of (lp)tBLMs, containing 750 nm radius defects.

Unaccounted Spectral Features. EI spectra in Figure 2 contain certain features that were not reproduced by FEA within the model framework currently used. In particular, curves of high defect density tBLMs in Figure 2c,d and tBLN systems in Figure 2g,h exhibit almost linear, often inclined by ~45° "tails", at the very low frequency end of the spectra. These parts of the spectra indicate that some very slow processes create an electrical bypass to a Helmholtz layer. Once the displacement current associated with the charging of the compact double layer becomes small enough due to their scaling as $1/\omega$, these processes manifest themselves as linear patches in the Cole−Cole plots. Because they slope upward with decreasing frequency, these processes must be related to phenomena other than charge displacement. It is quite possible that these features stem from the residual redox processes occurring at the interphase, such as reduction of dissolved oxygen or redox conversions of residual impurities in solution. These features most likely will depend on the ratio between the electron exchange rate and the diffusion. If the process is diffusion limited, one may expect a 45°

slope curve, whereas the slope will trend toward 90° for electron transfer limited. However, these surface processes cannot be modeled by the schemes shown in Figure 3.

Conclusions

The results of our work present evidence that, by varying simple experimental parameters, one may adjust both the morphology and dielectric properties/conductivity of tBLM systems. The cartoon in Figure 8 summarizes the general features of the qualitatively different surface constructs observed by AFM and studied by FEA, and the EIS provides valuable information to characterize such constructs. For example, spectral features of EI may serve as diagnostic tools for assessing the completeness or defectiveness of tBLMs.

FEA supported by AFM data demonstrates new possibilities to describe and predict EI spectra and their changes without referring to the equivalent circuit modeling, which frequently generates data difficult to associate with the physical parameters of the electrochemical systems. In contrast, FEA, in combination with the structural data from neutron reflectometry (layer thickness) and AFM (defect size), may generate quite realistic EIS plots, as seen in the Cole−Cole plots analyzed in this study.

Qualitative agreement observed between the predicted and experimental EI spectra supports the idea that not only may the major parameters of the tBLMs be extracted from the EI spectra but also important and sometimes unique information about the surface molecular architecture can be inferred. For example, a few nanometer size pinholes in tBLMs are invisible to most modern structural techniques, including AFM. Here we show by FEA that EIS unambiguously identifies such defects. In certain cases, the quantitative estimation of the surface coverage and/or the presence of three-dimensional (3D) objects such as bound liposomes may be tested via the analysis of the EI spectra. Such information may be useful in the studies, where the self-assembled tBLMs undergo time-dependent structural transformations.[23,26]

Finally, the qualitative agreement achieved here also acknowledges the limitations of the FEA used to model EI spectra. FEA was not able to predict certain features of the Cole−Cole plots. The very low frequency of EI spectra may not be accessible for FEA analysis at all, if they are related to the presence of residual redox species capable of exchanging electrons with the surface. In such cases, the lack of information about the nature and the properties of such species, as well as the lack of information on the rate constants of electron exchange may preclude application of FEA to EI response in this frequency range. Our modeling assumed surfaces to be homogeneous on both nano- and microscopic scale. This assumption is unlikely. Therefore, it is not surprising that the data presented in the current study demonstrate the limitations of such a simplified approach. Nevertheless, the ability of FEA to precisely predict major spectral features hints at the possibilities of utilizing this methodology to study much more complex systems, involving surface and bulk heterogeneity, complex defect size distributions, and various geometries.